2Pb5-4

Proceedings of Symposium on Ultrasonic Electronics, Vol. 32 (2011) pp. 265-266
8-10 November, 2011

Detection of Boundaries of Carotid Arterial Wall by Analyzing Ultrasonic RF Signals

超音波 RF 信号の解析による頸動脈壁の境界検出

Nabilah Ibrahim[1†], Hideyuki Hasegawa[2,1] and Hiroshi Kanai[1,2] ([1]Grad. School of Eng. Tohoku Univ.; [2]Grad. School of Biomed. Eng., Tohoku Univ.)
ナビラ　イブラヒム [1†], 長谷川英之 [2,1], 金井　浩 [1,2] ([1] 東北大院 工; [2] 東北大院 医工)

1. Introduction

Parallel to the fact that the IMT (Intima-Media Thickness) of the carotid arterial wall is most frequently used as the standard indicator to diagnose atherosclerosis [1], it is essential to accurately estimate the IMC (intima-media complex) boundaries, i.e., the LIB (lumen-intima boundary) and MAB (media-adventitia boundary). For the assessment of the accurate LIB and MAB positions, there is a technique using template matching between the adaptive model and the RF echo [2]. However, using this method, the negotiate errors between the adaptive model and the measured *in vivo* RF echo, and even between the adaptive model and the measured reference RF echo (echo from a point scatter) still occur. In [3], the template matching method was also reported for accurate estimation of the boundary, but it only detects the MAB. To overcome and/or reduce the drawbacks, first, we consider the improved-adaptive model to have the best fitting to the reference RF echo by improving the window function of the adaptive model in [2] with the Gaussian window. This is explained by the assumption that the ultrasonic (US) pulse is transmitted with a Gaussian envelope [4], and it retains the form during the propagation. Second, by applying the MSE (Magnitude Squared Error) method, we fitted the envelope of improved-adaptive model (multiply the sinusoidal wave with the Gaussian window) and the envelope of *in vivo* RF echo to estimate the boundaries, that will be explained below. In this paper, we estimated these boundaries positions accurately using the improved-adaptive model, and we showed the comparative results between this automated method and the manual method. We also showed that the improved-adaptive model gave better results than previous adaptive model, under the comparison to the results obtained manually.

2. Principle

2.1 Optimum Adaptive Model

Previous method [2] reported that the adaptive model has the best fit to the reference RF echo. However, there are still significant differences that would affect the boundaries detection. Therefore, we consider the parameter-adjustment of the adaptive envelope model signal $\hat{E}_x(n\mathrm{T_s})$ by multiply the sinusoidal wave $\hat{x}(n\mathrm{T_s})$ with the Gaussian window $w(n\mathrm{T_s})$ as follows:

$$\hat{E}_{xi}(nT_s) = \sqrt{\mathrm{Re}\{\hat{x}_i(nT_s)\}^2 + \mathrm{Im}\{\hat{x}_i(nT_s)\}^2}, \quad (1)$$

$$\hat{x}_i(nT_s) = a_i \cdot \sin[2\pi f_0(nT_s - \tau_i)] \cdot w_i(nT_s - \tau_i), \quad (2)$$

$$w_i(nT_s) = \frac{1}{\sqrt{2\pi\sigma^2}} \exp\left[-\frac{(nT_s - \mu)^2}{2\sigma^2}\right], \quad (3)$$

where center frequency f_0 = 7.5 MHz is set by estimating the peak frequency of the frequency spectrum obtained from the whole analyzed region, (n=1, 2 ,…, N-1) so that the best fit to the reference RF echo is obtained. In this report, the reference RF echo is the echo signal from a glass plate. a_1 and a_2 (i = 1: LIB, 2: MAB) are amplitude coefficients, and τ_1 and τ_2 are time delays of the LIB and MAB echoes, respectively. μ is the central time point of a constructed pulse, σ is the standard deviation of the Gaussian window $w(n\mathrm{T_s})$, which is determined so that the correlation between the envelope of the improved-adaptive model and the envelope of the echo from a glass plate (reference RF echo) is maximum. $\mathrm{T_s}$ is the sampling interval. Fig. 1 (left) shows the envelope of the improved-adaptive model with maximum correlation and the envelope of the echo from a glass plate. The correlation coefficient is 0.98, which is 4.1% higher than the maximum correlation (0.94) between the RF echo from a glass plate and the adaptive model (using Hanning window) (Fig. 1, right). Because of better accuracy, the envelope signal is considered in the fitting process.

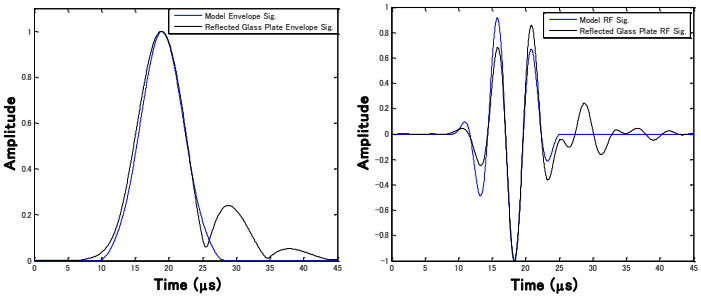

Fig. 1. Envelopes and RF reflected waveforms from a glass plate and model signal.

During the fitting process between the envelope of improved-adaptive model and the envelope of *in vivo* RF echo to estimate the boundaries, two envelopes of improved-adaptive models are combined instead of the envelope of combined the *in vivo* RF echoes, for modeling the echoes from LIB and MAB as shown in Fig. 2. Consequently, the envelope of the improved-adaptive model that is necessary to be fitted with the envelope of *in vivo* echo is defined as follows:

$$\hat{E}_x(nT_s) = \hat{E}_{x1}(nT_s) + \hat{E}_{x2}(nT_s), \quad (4)$$

where $E_{x1}(n\mathrm{T_s})$ and $E_{x2}(n\mathrm{T_s})$ are the envelope adaptive models of LIB and MAB, respectively.

2.2 Boundaries from the Manual Method

The red lines in the longitudinal B-mode image of the carotid artery posterior wall in Fig. 2 are the LIB and MAB marked manually. These boundaries are taken as

E-mail: nabilah@us.ecei.tohoku.ac.jp
(hasegawa, kanai)@ecei.tohoku.ac.jp

the base positions for the comparison with the automatic method results. However, since these boundaries are varies according to the operators, once, only the same operator is employed.

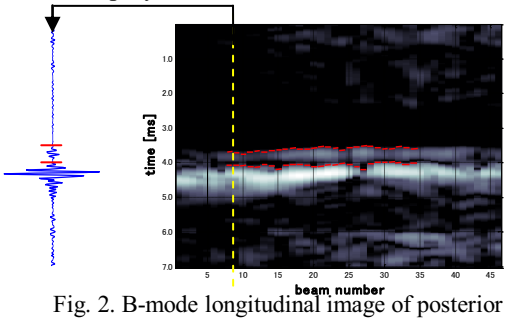

Fig. 2. B-mode longitudinal image of posterior carotid artery wall and echoes from the boundaries.

2.3 Accurate detection of the carotid artery boundaries

For the *in vivo* measurement, the ultrasonic machine (SSD-6500, ALOKA) was used. The right carotid artery of a healthy subject was scanned by a linear transducer, under the frequency of 10 MHz, and the RF echoes were acquired at a sampling frequency of 40 MHz.

For the evaluation of the detected LIB and MAB positions, the error α between the envelope of improved-adaptive model $\hat{E}_x(t)$ and the envelope of *in vivo* echo signal $E_x(t)$ is minimized by applying the MSE method.

$$\alpha(\tau_1,\tau_2)=\frac{1}{N}\sum_{i=0}^{N-1}\frac{\sum_{n=0}^{N-1}\left|E_x(nT_s)-\hat{E}_x(nT_s)\right|^2}{\sum_{n=0}^{N-1}\left|E_x(nT_s)\right|^2}. \quad (5)$$

Since the average IMT is ranged from 0.5 mm to 1.0 mm for a healthy person [5], and because the IMT is varies from person to person, this work scales the fitting region (corresponding to τ_2-τ_1) between 0.3 mm and 1.0 mm.

3. Results

An example of the normalized MSE distribution 10logα is shown in Fig. 3, indicating the positions of LIB and MAB (point P). Presenting the only 11% of α at this position would express that the improved-adaptive model is very good agreement with the measured *in vivo* envelope signal. The other data are also analyzed and the detected boundaries (red cross-lines) are shown in Fig. 4. Additionally, to have the better confirmation of the improved-adaptive model and used envelope signal, Fig. 5 shows the differences of boundaries positions detected between the automated method and the manual method for the beams of interest. Both the automated methods that using the envelope and the RF signal are employed the Gaussian window in adaptive model, in calculating the error α. The averages of the differences between these two methods for all beams are 1.1μm for using envelope and 1.2μm for using RF signal. There is no-difference occurred between these two automated methods for some beams, in the conjunctions of when comparing to the boundaries from manual method, the differences of the LIB and the MAB positions are equal to each other. Also, there are a few undesired results (8 beams) that the differences using the RF signals are smaller than using the envelope signals and the reason is still in consideration. However, for most of the beams, the results of using the envelope signals represent the smaller difference compared to the RF signal. This is clarified by the fact that the envelope of the improved-adaptive model is very good agreement to the envelope of the reference RF echo, which can be expressed by the approximate Gaussian envelope of US pulse.

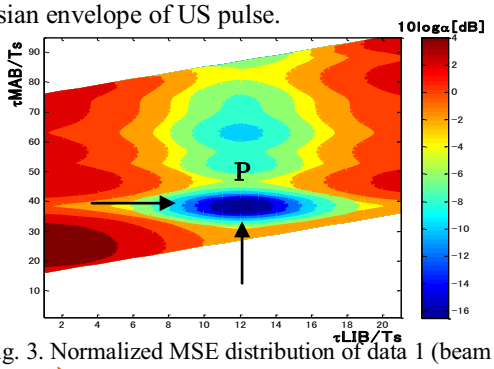

Fig. 3. Normalized MSE distribution of data 1 (beam 8).

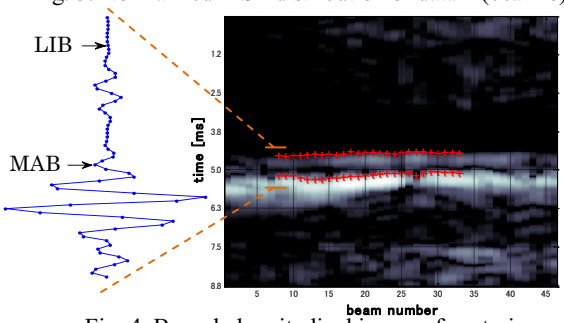

Fig. 4. B-mode longitudinal image of posterior carotid artery wall and enlarge of beam of interest echoes.

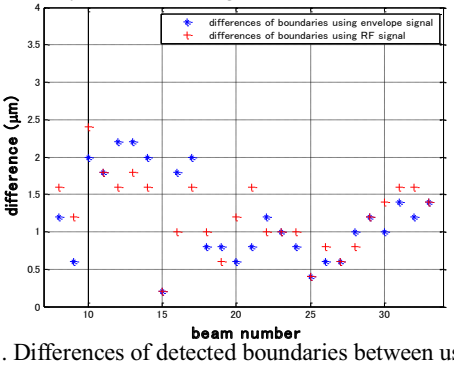

Fig.5. Differences of detected boundaries between using the envelope and the RF signal (automated) and manual method.

4. Conclusion

In this work, we accurately estimated the boundaries positions of IMC at the posterior wall of the carotid artery using the improved-adaptive envelope model signal and the measured *in vivo* envelope signal. The estimated boundaries were in good agreement with the results of the manual method, compared to the previous one.

References

[1] D. H. O'Leary: New Engl. J. Med. **340** (1999) 14.
[2] T. Kaneko, H. Hasegawa, and H. Kanai: Jpn. J. Appl Phys. **46** (2007) 4881.
[3] L. Fan, P. Santago, W. Riley, and D. M. Herrington: Ultrasound Med. Biol. **27** (2001) 399.
[4] L. Ferrari, and J. P. Jones: Ultrasound Med. Biol.**11**(2) (1985) 299.
[5] Japan Academy of Neurosonology **15**(2002) 20.